

# Timing properties and spectral states in Aquila X–1

P. Reig<sup>1</sup>, S. van Straaten<sup>2</sup>, M. van der Klis<sup>2</sup>

## ABSTRACT

We have analyzed five X-ray outbursts of the neutron-star soft X-ray transient Aquila X – 1 and investigated the timing properties of the source in correlation with its spectral states as defined by different positions in the color-color and hardness-intensity diagrams. The hard color and the source count rate serve as the distinguishing parameters giving rise to three spectral states: a low-intensity hard state, an intermediate state and a high-intensity soft state. These states are respectively identified with the extreme island, island and banana states that characterize the atoll sources. The large amount of data analyzed allowed us to perform for the first time a detailed timing analysis of the extreme island state. Differences in the aperiodic variability between the rise and the decay of the X-ray outbursts are found in this state: at the same place in the color-color diagram, during the rise the source exhibits more power at low frequencies ( $\lesssim 1$  Hz), whereas during the decay the source is more variable at high frequencies ( $\gtrsim 100$  Hz). The very-low frequency noise that characterizes the banana-state power spectra below 1 Hz cannot be described in terms of a single power law but a two-component model is required. In two outbursts a new 6-10 Hz QPO has been discovered and tentatively identified with the normal/flaring branch-like oscillation observed only at the highest inferred mass accretion rates. We have compared the spectral and timing properties of Aquila X – 1 with those of other atoll and Z sources. Our results argue against a unification scheme for these two types of neutron-star X-ray binaries.

*Subject headings:* accretion, accretion disks — stars: neutron — stars: individual (Aquila X–1) — X-rays: stars

---

<sup>1</sup>G.A.C.E, Instituto de Ciencias de los Materiales, University of Valencia, P.O. Box 22085, E - 46071 Paterna-Valencia, Spain

<sup>2</sup>Astronomical Institute “Anton Pannekoek”, University of Amsterdam and Center for High-Energy Astrophysics, Kruislaan 403, NL-1098 SJ Amsterdam, the Netherlands

## 1. Introduction

Aquila X – 1 belongs to the general group of systems known as low-mass X-ray binaries (LMXB). These systems consist of a neutron star or a black hole orbiting around a late-type star (later than A). The X rays are the result of the accretion of material from the companion onto the compact star. Mass transfer is thought to occur via Roche lobe overflow, and hence proceeds via an accretion disk. In Aquila X – 1, the compact star is a neutron star and the mass-donating companion is a V=21.6 K7V star, located at an estimated distance of 2.5 kpc (Chevalier et al. 1999). An orbital period of 18.95 hours has been suggested (Chevalier & Ilovaisky 1991; Welsh, Robinson & Young 2000). The high-energy radiation is characterized by 1.5–2 month long transient X-ray outbursts during which the X-ray luminosity can increase by more than three orders of magnitude. They are thought to be due to thermal instabilities in the accretion disk (e.g. van Paradijs 1996). Their recurrence time and duration vary but typical values are  $\sim 200$  days and 40–60 days, respectively (Šimon 2002). The source also displays Type I bursts (Zhang, Yu & Zhang 1998) that last a few tens of seconds and are interpreted as runaway thermonuclear burning of matter on the surface of the neutron star.

Various schemes have been proposed to categorize the LMXBs: X-ray spectral behavior as a function of intensity and the requirement of a low-energy black-body component in the X-ray spectra (Parsignault & Grindlay 1978; Naylor & Podsiadlowski 1993), cluster analysis of a large number of source characteristics (Ponman 1982), detailed X-ray spectral fits (White & Mason 1985), X-ray hardness-intensity and color-color diagrams (Schulz, Hasinger & Trümper 1989), aperiodic variability at very low frequencies (Reig, Papadakis & Kylafis 2003). Most relevant for the purpose of this paper is the classification scheme in terms of the rapid aperiodic variability and the patterns that these sources display in color-color diagrams (Hasinger & van der Klis 1989). In this scheme LMXBs are divided into two different subclasses, Z and atoll sources.

The three spectral branches that make up the Z shape are called horizontal branch, normal branch and flaring branch and the two structures that occur in atoll sources are known as the island and the banana (van der Klis 1989). At the lowest count rates an extension of the island state is sometimes seen with

a harder spectrum and stronger band-limited noise than the "canonical" island state (van Straaten, van der Klis & Méndez 2003 and references therein). The term *extreme island state* has been used to designate such state (Prins & van der Klis 1997; Reig et al. 2000). The spectral and timing properties of atoll sources in this state are reminiscent of those seen in the low/hard state of black hole systems (van der Klis 1994a, 1994b; Berger & van der Klis 1998; Olive et al. 1998; Belloni, Psaltis & van der Klis 2002). Both Z and atoll sources move through these patterns continuously, that is, without jumping from one branch to another, although the source motion along the spectral tracks is much slower in atoll sources when they are in the island state than in the banana state and in Z sources in all states. The classification of Aquila X–1 in this scheme was investigated by Reig et al. (2000) — see also Cui et al. (1998) —, who studied the correlated X-ray timing and spectral variations of Aquila X – 1 and presented evidence for its classification as an atoll source, exhibiting all classic atoll source states.

This scheme has been revisited by Muno, Remillard & Chakrabarty (2002) and Gierliński & Done (2002). They reported that three transient atoll sources which display a wide dynamic range in intensity ( $F_{max}/F_{min} \gtrsim 100$ ; 4U 1608–52, 4U 1705–44 and Aquila X – 1 trace out three-branch patterns in the color-color diagram similar to those of Z sources, and suggested this may be a general feature. Their study was based on the spectral properties only. However, as pointed out by Hasinger & van der Klis (1989) it is difficult to make a clear distinction between Z and atoll sources on the basis of the motion through the color-color diagram alone. Analysis of the rapid aperiodic variability to study the noise components in different regions of the color-color diagram and the actual time scales of the motion of the source through the diagram are important to identify source type and state.

In this work we have studied the spectral and timing properties of Aquila X – 1 in order to investigate whether atoll and Z sources can be unified into one classification scheme and provide new insights into the poorly known extreme island states of atoll sources. We find that although the color-color diagram shows a branch whose topology is similar to the normal branch of Z sources, neither the timing properties nor the motion in the color-color diagram of Aquila X – 1 agree with those of Z sources.

## 2. Observations

The data were retrieved from the *RXTE* archive and comprise all observations of Aquila X – 1 available from 1997 February to 2002 May. Data taken during satellite slews and Earth occultation were removed. Likewise, all Type I bursts were excluded from our analysis. The observations contain five X-ray outbursts. Although the duration and maximum intensity differ, the profile of the outbursts is very similar and is characterized by a fast rise and a slower decay. During intensity maximum the light curve is complex and multi-peaked. The fourth outburst showed two minor outbursts (the peak intensity was one order of magnitude lower than the main outburst) 70 days and 110 days after the main peak, respectively. The long-term light curve of the observations is shown in Fig. 1.

## 3. The color-color diagram

Background subtracted light curves corresponding to the energy ranges 2.0–3.5 keV, 3.5–6.0 keV, 6.0–9.7 keV and 9.7–16.0 keV were used to define the soft and hard colors as  $SC=3.5-6.0/2.0-3.5$  and  $HC=9.7-16.0/6.0-9.7$ , respectively. The color-color diagram (CD) of Aquila X – 1 was then constructed by plotting the hard color as function of the soft color (Fig. 2). During the time spanned by the observations the response of the detectors varied due to ageing. In addition, gain changes are applied occasionally, making the channel boundaries for a given energy range change with time, and also slightly affecting the effective areas of the detectors. Each gain change is the start of a new "gain epoch". We reduced the effect of the color shifts that results from these gain changes by linearly interpolating between the count rates in the two energy channels straddling the energy boundaries in each epoch. Each data point of Aquila X – 1 was normalized with the closest corresponding Crab point within the same gain epoch in order to mitigate the response change effects on the colors. The final CD was obtained by averaging the five (one for each detector) normalized CDs and rebinning into 256-s data points. We excluded data for which the resulting relative errors were larger than 5%. The total number of data points excluded from the analysis was  $\lesssim 10\%$ . In order to recover the true values of the colors of Aquila X – 1 the soft color should be multiplied by 2.35 and the hard color by 0.56 (quoted values are averages of the Crab colors during the observations and

for all five PCUs). The variation of the Crab colors computed as the root-mean-square, i.e. (the standard deviation over the mean color) was 5.3% and 1.7% for the soft and hard colors, respectively — see also Fig. 1 in van Straaten et al. (2003).

### 3.1. Spectral states

Aquila X – 1 can be found in two main states: a low-intensity hard state and a high-intensity soft state. In addition, a short-lived intermediate or transition state is found displaying values of the hard color in between the two main states. The aperiodic variability as a function of spectral hardness, i.e. position in the CD of Aquila X – 1 was previously studied by Reig et al. (2000). With only two of the five outbursts analysed in that work, the CD consisted of a soft branch, the banana branch, and two isolated groups of points which were called extreme island and island states. The large amount of data now analyzed reveals a more structured CD, in which the extreme island state appears as a more stable and longer-lived branch than the island state. The high/soft state corresponds to the classical banana state and the island state represents the transition between the two main states.

Outbursts 1, 4 and 5 (O1, O4 and O5) contain points in the two main states while outbursts 2 and 3 (O2 and O3) provide points to the banana state only. Observations of O2 and O3 began and finished when the source was still at a relatively high level of emission ( $> 1200$  c/s) and did not experience large amplitude changes ( $I_{max}/I_{min} < 5$ ). In contrast, outburst 1, 4 and 5 extended over a larger dynamic range in intensity ( $I_{max}/I_{min} > 50$ ). None of the points of the two minor outbursts which followed O4 (which will be termed here as O4') contributed to the banana state.

Outbursts 1, 4, 4' and 5 include points in the extreme island state. While O4 and O5 include points both during the rise and during the decay, O1 gives points during the decay only. The island state occurred only during the decay of O1 and O5. All five outbursts (except for O4') have points in the banana state but only O3 provides banana state points during the rise.

### 3.2. Motion in the color-color diagram

Figure 3 displays the motion of Aquila X – 1 in the CD for outbursts 4 and 5. Data points are  $\sim 1$ -day averages. Figure 4 shows the evolution of the colors

with time for those outbursts that include spectral transitions (O1, O4, O5). The 2–16 keV intensity just before the transitions is also given. All quoted intensities in this section are background subtracted and correspond to 5 PCUs in the energy range 2–16 keV. There is a strong correlation between the position of the source in the CD and its intensity. At the onset of the outbursts the data points distribute in the softest part of the extreme island state. The count rate is  $\lesssim 100$  c/s. As the intensity increases the source moves toward the right along the extreme island branch. The hard color (HC) slightly decreases on average. In about 6 days the count rate increases by one order of magnitude and the soft color (SC) increases by  $\approx +0.3$ . Then the source seems to jump to the banana state, recovering the initial values of the soft color. The hard color decreases by  $\approx -0.5$ . The 2–16 keV intensity is  $\sim 3$  or 4 times that of the extreme island state prior to the spectral transition, namely 4000–6000 c/s. No intermediate points between the two states are observed during the rise of the outbursts. This can be attributed to the fast rise and the lack of good sampling of the data. Indeed, the observational gaps between the last point of the extreme island branch and the first one of the banana branch were 2.6 and 3.1 days for O4 and O5, respectively.

As the intensity continues to increase the source becomes harder, i.e., it moves to the right along the banana, with approximately constant hard color. The peak of the outburst is characterized by flaring activity with erratic changes in count rate. The count rate at the peak is 50–100 times the minimum detected count rate. Despite this irregular behavior the correlation between the intensity and the colors is maintained in the sense that the lower intensity points in the flares display a lower soft color as it is illustrated in Fig. 5. In other words, during the flare maxima the source lies at the right end of the banana branch, and in between flares it moves to the left. Thus the flaring variability in the light curve translates into the CD in a back and forth motion which approximately extends over the right half part of the banana state. This motion is quite fast. As an example, in one of the flares in O5 the soft color changed by 0.08 in about 2.4 hr. In another flare by 0.06 in 0.55 hr. This flaring behavior is seen in all outbursts but O2 shows it exclusively (Fig. 5). Such behavior stops once the source gets to half way the decay of the outburst, at which point the source shifts to lower soft colors (to

the left along the banana branch).

As the outburst declines the source moves back along the banana branch, abandoning it when the count rate becomes lower than  $\sim 800$  c/s. The transition to the hard state occurs at much lower soft color than when it entered the banana, although not necessarily at the lowest soft color. The banana state covers values of the soft color between 0.87 (O5) and 1.16 (O3). The transition to the hard state takes place at  $SC \approx 0.92$ – $0.93$  (Fig. 3). The count rate at which the transition between the two main states takes place is higher when the source is in the rise of the outburst. Hard to soft transitions occur when the count rate is well above  $\sim 1000$  c/s. Soft to hard transitions when the count rate is well below  $\sim 1000$  c/s as it can be seen in Fig. 4.

Rather than jumping directly to the hard branch the source remains for a short time ( $\leq 0.1$  days) in an intermediate state, the island state. Note that such a short island state episode would usually have been missed due to data gaps in the rise. The count rate in the island state is  $\sim 200$ – $400$  c/s. At even lower count rates the source finds itself back in the extreme island branch, moving toward the left as the intensity decreases, to eventually become too weak to measure the colors sufficiently well. The source re-enters this state during the decay when the count rate goes below  $\sim 200$  c/s. The re-entry point occurs at a lower soft color ( $SC \approx 1.05$ – $1.10$ ) then when the source left the extreme island state ( $SC \approx 1.3$ ). As the speed of motion along the extreme island state is approximately constant, the time during which the source can be found in this state is shorter during the decay of the outburst than during its rise. A difference in the position of the source in the CD depending on whether the source intensity increases or decreases was already recognized by Reig et al. (2000).

The main result that should be stressed is that transitions between states do not occur at the same point of the spectral branches. During the rise of the X-ray outburst the source occupies the hardest parts of the extreme island state before the spectral transition to the banana state. During the decay it tends to occupy the softest part of the banana branch before moving into the island state. However, the points of departure and arrival are different. In the CD, this translates into some sort of rectangular track (Fig. 3) along which Aquila X – 1 moves clockwise as the count rate first increases and then decreases.

In addition to Fig. 4, Tables 1 and 2 also illustrate

the time scale for the motion through the diagram. Table 1 and Table 2 give upper limits on the duration of the source in each state and the time scales of the spectral transitions, respectively. Note that the observational gap for the spectral transitions from the extreme island state to the banana state is approximately two times longer than viceversa. Given the speed of motion of the soft color along the extreme island branch (roughly  $0.05 \text{ day}^{-1}$ ) a three-day gap might imply a change in soft color of about 0.15. Thus, it is possible that the actual entry point into the banana branch is at lower values of the soft color. In this case the motion of Aquila X – 1 in the CD would be similar to that of 4U 1705-44 (Barret & Olive 2002), in which both the transition from (to) the extreme island state to (from) the banana state occur at the same point of the banana branch. The motion in the CD then would then resemble an inverted triangle rather than a rectangle.

#### 4. Timing analysis

In order to investigate the aperiodic variability of Aquila X – 1 we obtained power spectra by dividing the 2–60 keV PCA data of each observation into 256-s segments and calculated the Fourier power spectrum of each segment up to a Nyquist frequency of 2048 Hz. The high-frequency end (1500–2048 Hz) of the power spectra was used to determine the underlying Poisson noise (approximated by a constant power level), which was subtracted before performing the spectral fitting. Our aim is to investigate the aperiodic variability in correlation with the spectral states, which in turn, correlate with the source count rate. Thus we divided the color-color plane into various regions and obtained a mean power spectrum for each region. The mean power spectrum was the result of averaging all the power spectra corresponding to the points enclosed in each color region. See Table 3 to find the average values of the colors, boundaries and intensity of each region. Prior to this, we investigated whether power spectra from the same CD region taken at different outbursts were consistent with having the same properties. We found that while this was true for the banana state, some differences existed in the extreme island state depending on whether the source was in the rise or the decay of the X-ray outburst.

The extreme island state is populated with points from the rising part of O4 and O5, the decaying part of O1, O4 and O5 and from the extended extreme is-

land state of O4'. Consequently, the extreme island state was first separated into points pertaining to the rise, to the decay or to O4'. Then each one of these groups was further divided into three subgroups according to the value of the soft color. Note that in the case of the rise and decay regions this division implies a division in count rate as well as in hard color. On average, the extreme island states EISrise1 and EISdecay2, (see Table 3) have lower intensity and are softer than EISrise2 and EISdecay1, respectively. In turn, EISrise2 contains softer points than EISrise3. The island state points (intermediate state) defined another region. The timing properties of the banana state in atoll sources have been seen to vary smoothly as the soft color, or equivalently, the count rate increases, that is, from the lower (left) to the upper (right) banana branch. Therefore, the banana branch was split into five regions (BS1 to BS5) in increasing order of the soft color. Each region approximately contains the same amount of data.

There is no unanimity in the literature about the names of the power spectral noise components nor about the mathematical functions used to fit those components. In this work we have followed the terminology of Belloni et al. (2002) and fitted the power spectra using Lorentzian functions only. Also, for displaying our power spectra we have used the power times frequency representation  $\nu \times P(\nu)$  vs  $\nu$ , in which the product of the power density in the rms normalization and the Fourier frequency is plotted as a function of the Fourier frequency (Belloni et al. 1997). As fit parameters we use the frequency  $\nu_{\text{max}}$  at which the Lorentzian attains its maximum value in such representation, and the  $Q$  value, which gives a measure of the coherence of the Lorentzian. In terms of the half width at half maximum or  $\Delta$ , these quantities are related by  $\nu_{\text{max}} = \sqrt{\nu_0^2 + \Delta^2}$  and  $Q = \nu_0/2\Delta$ , where  $\nu_0$  is the central frequency of the Lorentzian. Between three and five Lorentzians were needed in order to get a good fit. If during the fitting procedure a Lorentzian component resulted with negative  $Q$  value then we set it to zero.

It should be noted that the naming scheme of Belloni et al. (2002) was applied, in the case of low-luminosity neutron stars, to systems displaying the island state only. Thus, a complete description of some power spectra, especially those in the banana state, in terms of the noise components given in that work is not always possible and extra or new components are needed in order to obtain acceptable fits.

The extensions to the Belloni et al. naming scheme we use are those of van Straaten et al. (2003).

In the terminology of Belloni et al. (2002), the band-limited noise of atoll sources in the (extreme) island state consists of three Lorentzians namely,  $L_b$  that accounts for the power spectrum at low frequencies ( $\lesssim 1$  Hz),  $L_\ell$  and  $L_u$  that fit its high-frequency end.  $L_\ell$  may show up as a broad bump at frequencies 10–25 Hz (normally in the island state) or as a narrow QPO at frequencies  $\gtrsim 100$  Hz (normally in the banana state). In fact, at frequencies above  $\gtrsim 100$  Hz  $L_\ell$  and  $L_u$  represent the kHz QPOs seen in low-mass X-ray binaries. However, note that this identification of  $L_\ell$  with both a broad peak and the lower kHz QPO is only tentative and the broad bump at 10–25 Hz might alternatively represent a separate component (van Straaten et al. 2002). The intermediate frequency range (1–100 Hz) is described by one broad Lorentzian or "hump",  $L_h$  and one narrow Lorentzian  $L_{LF}$  referred to as the low-frequency QPO. Not detected by Belloni et al. (2002) but also present in some atoll sources (van Straaten et al. 2002) is the so-called hectoHerz QPO,  $L_{hHz}$ , a broad feature with characteristic frequency at  $\sim 100$  Hz.

#### 4.1. Spectral states: aperiodic variability

Table 4 lists the results of the fits and Fig. 6 depicts the power spectra and fit functions for different regions of the CD (see Table 3 to identify the position in the CD).

##### 4.1.1. The extreme island state (EIS)

The extreme island state power spectrum contains, in order of increasing frequency, the low-frequency band-limited noise,  $L_b$ , the broad peak low-frequency noise  $L_h$ , the broad version of  $L_\ell$  and one more component which could be either the hHz QPO or a kHz QPO. Based on the rms/frequency correlations of the noise components seen in other atoll sources, van Straaten et al. (2002, 2003) favored the upper kHz interpretation. If  $L_\ell$  is also interpreted as the lower kHz QPO then the intervals EISrise2, EISrise3 and ISO4<sub>2</sub>' (see Fig.6) would represent the first detection of the two kHz QPO in Aquila X – 1. Alternatively, the fourth component could be the hHz QPO. Note that the narrow  $\sim 1160$  Hz peak in EISO4<sub>2</sub>' is not statistically significant. An F-test reveals that the probability that the improvement of the fit (in terms of a lower  $\chi^2$ ) by the addition of an extra Lorentzian

happen by chance is larger than 30%. The characteristic frequencies of the noise components increase and their rms values decrease slightly as the count rate increases, i.e., the source moves toward the right in the extreme island state.

Figure 7 displays the characteristic frequency of the  $L_h$  and  $L_\ell$  components as a function of the band-limited noise component  $L_b$  for Aquila X – 1, the atoll sources 4U 1608–52 (van Straaten et al. 2003), 4U 1728–34 and 4U 0614+09 (van Straaten et al. 2002) and the Z source GX5–1 (Jonker et al. 2002). In the case of GX5–1 the horizontal branch oscillation is plotted instead of  $L_h$ . Note also that the broad-band noise in the Z source was not fitted with a Lorentzian but with a cutoff power law,  $P(\nu) \propto \nu^{-\alpha} e^{-\nu/\nu_{cut}}$ . By differentiating  $\nu P(\nu)$  and equating the resulting function to zero the maximum frequency of the Z band-limited noise,  $\nu_{max} = (1 - \alpha)\nu_{cut}$ , was derived. Figure 7 seems to confirm that *i*) the 1–20 Hz broad feature  $L_h$  observed in atoll sources at low count rates (island states) has the same origin as the horizontal branch oscillations (HBO) observed in Z sources (Psaltis, Belloni & van der Klis 1999, van Straaten et al. 2003), *ii*) the broad bump at frequencies 10–25 Hz is associated with the lower kHz QPO. The extreme island state data in Aquila X – 1 sample the lowest characteristic frequencies so far detected.

One interesting result from the timing analysis of the extreme island state is the differences in the aperiodic variability of the source during the rise and decay of the outbursts. Figure 8 shows three power spectra of Aquila X – 1 and an enlargement of the CD displaying the extreme island state. All three power spectra are associated with the same value of the colors, i.e, they occupy the same position in the CD (marked in Fig. 8). However, they correspond to different parts of the X-ray outburst: rise (diamonds), decay (stars) and when the source found itself in the extended island state of O4' (crosses). During the rise the power is concentrated at low frequencies whereas during the decay, the source exhibits more power at high frequencies. During the extended island state of outburst O4' there is roughly equal power at all frequencies. The differences in the characteristic frequencies of the noise components are much less pronounced and consistent with one another whenever the same component appears.

#### 4.1.2. The banana state

The low-frequency end ( $\lesssim 1$  Hz) of the banana state power spectra is dominated by the very-low frequency noise (VLFN). One single power law is normally used to fit this component. However, the power spectrum of Aquila X – 1 below 1 Hz cannot be described by one component only. In order to fit the VLFN we used two zero-centered Lorentzians that were called low VLFN ( $L_{LVLFN}$ ) and high VLFN ( $L_{HVLFN}$ ) (Schnerr et al. 2003). The characteristic frequencies of these components are found to be independent of the position of the source in the CD:  $\nu_{\max} \sim 0.01$  Hz and  $\sim 0.03$  Hz, respectively. However, while the fractional rms variability of lower frequency VLFN roughly remains constant at  $\sim 3.4\%$ , the higher frequency VLFN becomes stronger — increasing from  $\sim 0.9\%$  in the lower banana to  $\sim 2\%$  in the upper banana — as the count rate increases.

Above 1 Hz the banana state power spectra contain one broad Lorentzian, describing the band-limited noise and one QPO (two in BS1). The characteristic frequency and width of the broad band-limited noise component decrease as the count rate increases (i.e. as the source moves toward the right). This component has also been seen in 4U 1608–52 (van Straaten et al. 2003), 4U 0614+09 and 4U 1728–34 (van Straaten et al. 2002). However, the lack of data precludes a more detailed comparison. Only 4U 1728–34, with just two measurements, seems to have the same behavior as Aquila X – 1 i.e., the frequency of this noise component decreases along the banana. Following van Straaten et al. (2003) we will refer to this component as  $L_{b2}$ . Next to, sometimes on top of, the band-limited noise in the banana state there is a relatively narrow peak, whose characteristic frequency and width do not correlate with any other parameter. This narrow QPO has a frequency in between that of the hHz Lorentzian and  $L_h$ . van Straaten et al. (2003) — see also di Salvo et al. (2001) and van Straaten et al. (2002) — argued that it is the band-limited noise component  $L_b$  which transforms into a narrow QPO above certain frequency ( $\sim 20$  Hz in 4U 1608–52). The appearance of  $L_{b2}$  and this transformation of  $L_b$  occurs coincidentally. In Aquila X – 1, although the narrow version of  $L_b$  appears systematically in all banana-state power spectra it is always below  $3\sigma$ .

The detection of a second kHz QPO in Aquila X – 1 is only marginal (van der Klis 2000). Based on

the values of the fitting parameters and the relation between the QPO frequency and the X-ray colors, Méndez, van der Klis & Ford (2001) concluded that whenever a kHz QPO is detected in Aquila X – 1 it is always the lower kHz QPO. The fractional rms and characteristic frequency of the second QPO in BS1 are consistent with being the lower kHz QPO (Fig. 1 of Méndez, van der Klis & Ford 2001). Also, the characteristic frequencies of the  $L_\ell$  and  $L_b$  in BS1 agree with the correlation of Fig. 7 if an extrapolation to higher frequencies of the Aquila X – 1 points is done.

#### 4.1.3. The island state (IS)

The analysis of the transition state is hampered by poor statistics given the relatively low number of points. One single Lorentzian with peak at  $\approx 20$  Hz and  $Q$  value of 0.15 accounts for the entire 0.01–100 Hz frequency band. This noise component is identified as  $L_b$ . A second narrower Lorentzian with  $\nu_{\max} \approx 710$  Hz and  $Q \approx 3$  fits the noise at higher frequencies. Its fractional rms,  $\sim 17\%$ , is too high to agree with the lower kHz QPO. In fact, the value of the frequency and rms are similar to what it is seen in 4U 1608–52 and 4U 1728–34 for the upper kHz QPO (Fig. 1 of Méndez, van der Klis & Ford 2001). Nevertheless, given the relatively noisy spectrum at high frequencies such identification should be taken with care.

### 4.2. The normal/flaring branch-like oscillations

A QPO with frequency 7–14 Hz has been found in at least two atoll sources, XTE J1806–246 (Wijnands & van der Klis 1999; Revnivtsev, Borozdin & Emelyanov 1999) and 4U 1820–30 (Wijnands et al. 1999). These QPOs are detected at the highest inferred mass accretion rates only, are short-lived (a few hundreds of seconds) and are localized in a very narrow region of the CD, namely the tip of the upper banana. They are reminiscent of those observed in Z sources in the normal and flaring branches, when the source is accreting near the Eddington limit. Thus the detection of similar QPO in atoll sources at significantly lower accretion rates questions the current models that explain NBO in terms of near-Eddington accretion (Fortner, Lamb & Miller 1989). We searched for NBO-like QPO in Aquila X – 1 and tentatively found two of them at  $\sim 3\sigma$  significance, at frequencies  $10.3 \pm 0.5$  Hz in O3 and  $5.8 \pm 0.2$

Hz in O5 (Fig. 9). They have similar rms amplitude ( $\approx 0.7\%$ ) and Q-values ( $\approx 3$ ). The average values of the colors and intensity associated with these QPOs are SC=1.11, HC=0.52,  $I_X=5045$  count  $s^{-1}$  and SC=1.06, HC=0.51,  $I_X=6870$  count  $s^{-1}$ , respectively. For the sake of comparison with other sources we also give the value of the X-ray luminosity:  $8.5 \times 10^{36}$  erg  $s^{-1}$  for outburst 3 and  $8.1 \times 10^{36}$  erg  $s^{-1}$  for outburst 5. As a confirmation that they occur at the highest count rates, typical luminosities in the softest parts of the extreme island and banana states are  $3 \times 10^{34}$  and  $2 \times 10^{36}$  erg  $s^{-1}$ , respectively. The values of the luminosity are for a distance of 2.5 kpc and the energy range 2–16 keV. In the other three outbursts the detection is only marginal. The low statistical significance of these QPOs ( $\lesssim 2.5$ ) can be ascribed to their extremely short life.

## 5. Discussion

We have analysed all the available RXTE data of Aquila X – 1 between 1997 February and 2002 May and investigated its spectral and timing properties in correlation. This work has been motivated by recent reports that show that if large data sets are used, the atoll sources displaying the largest amplitude variations in intensity show three-branch patterns in the color-color diagram (CD), reminiscent of Z sources (Muno, Remillard & Chakrabarty 2002; Gierliński & Done 2002). Consequently, they conclude that the distinction between atoll and Z sources might be no longer justified. The extended island state, island state and banana state of atoll sources would then correspond to the horizontal branch (HB), normal branch (NB) and flaring branch (FB), respectively. The results of these studies were based on the spectral properties (i.e. color-color diagram) only. In order to be able to distinguish between the different types of low-mass X-ray binaries the rapid aperiodic variability associated with the various spectral states needs to be addressed as well (Hasinger & van der Klis 1989), and that is what we have attempted in this paper. We first make a comparison of the timing properties of Aquila X – 1 with those of other atoll sources and then discuss whether or not it can be considered as a Z source.

### 5.1. Comparison with atoll sources

4U 1608–52 and Aquila X – 1 are the atoll sources that display the largest dynamic range in X-ray in-

tensity ( $I_{max}/I_{quiescence} > 1000$ ). Thus a comparison between these two sources is of particular interest. 4U 1608–52 has been extensively studied by van Straaten et al. (2003). By comparing the shape of the power spectra (see Fig. 7 in van Straaten et al. 2003 and our Fig. 6) and the results of the power spectral fits (their Table 2 and 3 and our Table 4) one can find distinct similarities between the two sources: the power spectra of intervals A, B and C in 4U 1608–52 resemble those of the extreme island state of Aquila X – 1, while interval D of 4U 1608–52 is reminiscent of the island state in Aquila X – 1. Likewise, the shape and number of Lorentzians appearing in the power spectra of the extreme island state of Aquila X – 1 are similar to those of the three low-luminosity X-ray bursters studied by Belloni et al. (2002).

It is worth noting the relevant role of the hard color in connection with the timing properties of the extreme island state. In Aquila X – 1 the characteristic frequencies of the timing features in the extreme island state increase from left to right. This is opposite to what it is seen in 4U 1608–52, where frequencies increase from right to left. However, in both sources the increase in frequencies occurs in correlation with an overall decrease in hard color. We therefore suggest that in the extreme island state it is the hard color, rather than the intensity, which is the main determining factor of the timing properties. We note, that black hole candidates are likewise characterized by power spectral states whose occurrence seems to primarily depend on spectral hardness and which are relatively insensitive to intensity, and which are associated with two-dimensional motion through the color-intensity plane rather than motion along a one-dimensional track (Homan et al. 2001). It may be that in the island and extreme island states, the states in which atoll sources are most similar to black holes (e.g., van der Klis 1994a; Belloni, Psaltis & van der Klis 2002), possibly because in these states the inner disk radius is furthest from the neutron star surface, this 2-D picture better describes neutron star behavior than the 1-D description appropriate to the banana state and to Z sources.

Leaving aside the kHz QPOs, the overall shape of the banana-state power spectra of Aquila X – 1 present similarities with those of other atoll sources, namely, a strong red-noise component, the very-low frequency noise (VLFN) below  $\sim 1$  Hz and a broad and a narrow components describing the band-limited noise (BLN) in the frequency range 1–100 Hz. Com-



pared to 4U 0614+09, 4U 1608-52 and 4U 1728-34, Aquila X - 1 exhibits the strongest VLFN but the weakest BLN. While the VLFN is normally described by either a power law with index between 1.5-2.0 or a zero centered Lorentzian in the other atoll sources, it requires the use of two model components in Aquila X - 1, similar to the case of GX 13+1 (Schnerr et al. 2003). The broad band-limited noise component  $L_{b_2}$  in Aquila X - 1 and 4U 1608-52, or equivalently the zero centred Lorentzian in 4U 1728-34 and 4U 0614+09 have similar rms values. In contrast,  $L_b$ , which is clearly detected in these other atoll sources, is not significant in Aquila X - 1 in the banana state.

## 5.2. Is Aquila X - 1 a Z source?

Gierliński & Done (2002) suggested that the name atoll source is no longer appropriate as these type of low-mass X-ray binaries also display a three-branch pattern in the color-color diagram when large data sets of observations are used, reminiscent of the Z pattern for which Z sources are named. This effect is more pronounced in systems exhibiting large flux variations (Muno et al. 2002), like Aquila X - 1. The CD of Aquila X - 1 (Fig. 2) does indeed show a branch (the island state) that can be interpreted to connect the two main branches like in a Z shape. In addition, the correlation between the characteristic frequency of the 1-20 Hz broad Lorentzian  $L_h$  and the band-limited noise component (Fig. 7) at low count rates, suggesting a common origin with the horizontal branch oscillations and LFN in Z sources and the discovery of 7-14 Hz QPO at the highest X-ray flux (Fig. 9), reminiscent of the Z-source normal/flaring branch oscillations, strengthen the similarities between Aquila X - 1 and Z sources.

However, there are a number of systematic differences that clearly puts Aquila X - 1 outside the group of Z sources. First, there is the motion in the CD. In the extreme island state as the count rate increases the soft color increases and the hard color decreases. Then the source makes a rapid transition to the banana state and proceeds to harder colors (right) as the count rate increases further. However, after the peak of the outburst, when the intensity decreases the source does not follow exactly the reverse path. As shown in Fig. 3, Aquila X - 1 enters the banana state (extreme island state) at a higher (lower) value of the soft color than when it leaves it. The source moves clockwise following a rectangle track. It should be

pointed out that the entrance into the banana state at such high soft color is not caused by the time resolution used ( $\sim 1$  day) in Fig. 3. A 256-s bin shows the same effect. However, we cannot rule out an observational origin since the time gap between the transition from the extreme island state to the banana state is  $\approx 5$  days for outburst 5 and  $\approx 2.6$  for outburst 4 (Table 2). If this is the case and the source entered the banana state from the left then the pattern that it would trace out in the CD would be that of an inverted triangle, much like 4U 1705-44 (Barret & Olive 2002). In contrast, the re-entrance into the extreme island state at a low soft color is probably not caused by the lack of data given the relatively short gap between the island state and the extreme island state (just 1.6 days in outburst 5). In either case this behavior is not that of Z sources. In Z sources, the NB is not a fast transition between the other two branches, and the source follows the same path whether it is going up or down along the NB. In this respect, Aquila X - 1 is like the other two atoll sources that display high-amplitude flux variations. More detailed looks into the motion of 4U 1608-52 and 4U 1705-44 have revealed different topologies from the classical Z-shaped track. The motion of 4U 1608-52 resembles the greek letter  $\epsilon$  (van Straaten et al. 2003) and 4U 1705-44 describes an inverted triangle (Barret & Olive 2002). As noted above, these various topologies may simply be different aspects of 2-D motion through the color-intensity plane in which it is hard color that determines the timing properties.

Second, the amplitude of the X-ray luminosity change over the Z track is also different. In Aquila X - 1 the X-ray luminosity throughout the CD, i.e., from the left of the banana state to the right of the extreme island state is about three orders of magnitude. In Z sources, luminosity changes are typically less than a factor of 2 (di Salvo et al. 2000, 2001, 2002).

Third, another difference is the velocity and time spent by the source in each spectral state. Jonker et al. (2002) calculated that the Z source GX 5-1 spent most of the time in the normal branch. In contrast, Aquila X - 1 spends the smallest percentage of the the total observing time in the transition state (the analogue to the normal branch would Aquila X - 1 be a Z source). Wijnands et al. (1997) found that Cyg X-2 moves through the Z most slowly on the HB, faster on the NB and fastest on the FB. During a typical X-ray outburst, i.e., when Aquila X - 1 is X-ray active, it spends most of its time in the banana

branch (the analogue to the flaring branch).

Finally, the properties of the aperiodic variability of Aquila X – 1 also differ from those in Z sources, especially at very low count rates. We can establish the following differences:

- The very existence of the extreme island state. Although the characteristic frequencies in Aquila X – 1 increase along the extreme island state as the count rate increases as Z sources do in the HB, the latter never reach the low frequencies that are seen in atoll sources in the extreme island state, even when at the left end of the HB. Likewise, the rms amplitude of the noise components in the extreme island state is significantly higher than in a Z source HB. The total rms amplitude of those components in Aquila X – 1 amounts to  $\sim 30\%$ , while typically in Z sources, it does not go above  $\sim 10\%$ . The extreme island-state power spectra are typical of atoll sources.
- The peaked noise components, such as  $L_h$  and the upper kHz QPO are narrow QPOs on the HB in Z sources, with typical values of the Q parameter above 3 for the upper kHz QPO, whereas they are considerably broader peaked noise components in the extreme island state in Aquila X – 1 ( $Q < 0.5$ ).
- In Aquila X – 1, the normal/flaring branch-like oscillation does not occur during the "normal/flaring branch", i.e. the island or the lower banana branches but in the upper banana branch, just like in other atoll sources.
- The strength of the kHz QPOs decreases as the Z source moves along the Z track from HB to NB. Typically, the kHz QPOs become undetectable by the time the source reaches the middle of the NB. In contrast, Aquila X – 1 presents kHz QPOs in the island and banana states.
- The time scales of the aperiodic variability tend to decrease (frequencies increase) as the Z source moves along the FB, which is the opposite behavior to what is observed in Aquila X – 1 in the banana branch.

## 6. Conclusions

We have investigated the timing and spectral properties of the soft X-ray transient Aquila X – 1 during

five X-ray outbursts covering a period of more than five years. Three spectral states show up in the color-color diagram of Aquila X – 1: a low/hard state, identified with an extreme island state, a high/soft state corresponding to the classic banana state and an intermediate state associated with the island state of atoll sources. We have found that the hard color plays a crucial role in determining the timing properties of the extreme island state. Although the overall distribution of these states in the color-color diagram may resemble a Z, neither the motion in the CD, nor the typical time scales through the different branches of the CD, nor the range of X-ray luminosities, nor the timing properties at very low count rates (the existence of the extreme island state) are compatible with the classical Z-source behavior.

PR is a researcher of the programme *Ramón y Cajal* funded by the University of Valencia and the Spanish Ministry of Science and Technology. PR also wants to thank the University of Crete for providing in part the resources needed to carry out this work. This research has made use of data obtained through the High Energy Astrophysics Science Archive Research Center Online Service, provided by the NASA/Goddard Space Flight Center.

## REFERENCES

- Barret, D. & Olive, J.F., 2002, *ApJ*, 576, 391
- Belloni, T., van der Klis, M., Lewin, W. H. G., van Paradijs, J., Dotani, T., Mitsuda, K., & Miyamoto, S., 1997, *A&A*, 322, 857
- Belloni, T., Psaltis, D., van der Klis, M., 2002, *ApJ*, 572, 392
- Berger, M., & van der Klis, M., 1998, *A&A*, 340, 143
- Chevalier, C. & Ilovaisky, S. A. 1991, *A&A*, 251, L11
- Chevalier, C., Ilovaisky, S.A., Leisy, P., Patat, F., 1999, *A&A*, 347, L51
- Cui, W., Barret, D., Zhang, S.N., Chen, W., Boirin, L., Swank, J., 1998, *ApJ*, 502, L49
- Di Salvo, T., Stella, L., Robba, N. R., van der Klis, M., Burderi, L., Israel, G. L., Homan, J., Campana, S., Frontera, F., Parmar, A. N., 2000, *ApJ*, 544, L119
- di Salvo, T., Méndez, M., van der Klis, M., Ford, E., Robba, N. R., 2001, *ApJ*, 546, 1107
- di Salvo, T., Farinelli, R., Burderi, L., Frontera, F., Kuulkers, E., Masetti, N., Robba, N. R., Stella, L., van der Klis, M., 2002, *A&A*, 386, 535
- Fortner, B., Lamb, F. K., Miller, G. S., 1989, *Nature*, 342, 775
- Gierlinski, M., Done, C., 2002, *MNRAS*, 331, L47
- Hasinger, G. & van der Klis, M. 1989, *A&A*, 225, 79
- Homan, J., Wijnands, R., van der Klis, M., Belloni, T., van Paradijs, J., Klein-Wolt, M., Fender, R., Méndez, M., 2001, *ApJS*, 132, 377
- Jonker, P. G., van der Klis, M., Homan, J., Méndez, M., Lewin, W.H.G., Wijnands, R., Zhang, W., 2002, *MNRAS*, 333, 665
- Méndez, M. van der Klis, M., Ford, E.C., 2001, *ApJ*, 561, 1016
- Muno, M.P., Remillard, R.A., Chakrabarty, D., 2002, *ApJ*, 568, L35
- Naylor, T., Podsiadlowski, Ph, 1993, *MNRAS*, 262, 929
- Nowak, M.A., 2000, *MNRAS*, 318, 361
- Olive, J. F., Barret, D., Boirin, L., Grindlay, J. E., Swank, J. H., & Smale, A. P. 1998, *A&A*, 333, 942
- Parsignault, D.R., Grindlay, J.E., 1978, *ApJ*, 225, 970
- Ponman, T, 1982, *MNRAS*, 200, 351
- Prins, S., van der Klis, M., 1997, *A&A*, 319, 498
- Psaltis, D., Belloni, T., van der Klis, M., 1999, *ApJ*, 520, 262
- Reig, P., Méndez, M., van der Klis, M., Ford, E. C., 2000, *ApJ*, 530, 916
- Reig, P., Papadakis, I., Kylafis, N., 2003, *A&A*, 398, 1103
- Revnivtsev, M., Borozdin, K., Emelyanov, A., 1999, *A&A*, 344, L25
- Schnerr, R.S., Reerink, T., van der Klis, M., Homan, J., Méndez, M., Fender, R.P., & Kuulkers, E., astro-ph/0305161
- Schulz, N. S., Hasinger, G. & Trümper, J. 1989, *A&A*, 225, 48
- Šimon, V., 2002, *A&A*, 381, 151
- van der Klis, M., 1989, *ARA&A*, 27, 517
- van der Klis, M, 1994a, *A&A*, 283, 469
- van der Klis, M, 1994b, *ApJS*, 92, 511
- van der Klis, M., 2000, *ARA&A*, 38, 717
- van Paradijs, J., 1996, *ApJ*, 464, L139
- van Straaten, S., van der Klis, M., di Salvo, T., Belloni, T., 2002, *ApJ*, 568, 912
- van Straaten, S., van der Klis, M., Méndez, M., 2003, *ApJ*, in press, astro-ph/0307041
- Welsh, W.F., Robinson, E.L., Young, P., 2000, *AJ*, 120, 943
- White, N.E., Mason, K.O., 1985, *SSRv*, 40, 167
- Wijnands, R., van der Klis, M., 1997, *ApJ*, 482, L65
- Wijnands, R., van der Klis, M., 1999, *ApJ*, 514, 939
- Wijnands, R., van der Klis, M., Rijkhorst, E. 1999, *ApJ*, 512, L39

Zhang, S. N., Yu, W. & Zhang, W., 1998, ApJ, 494,  
L71

TABLE 1  
DURATION AND INTENSITY (2–16 keV, 5 PCUs) OF THE SPECTRAL STATES FOR EACH OF THE FIVE X-RAY  
OUTBURSTS

States	Duration days	I <sub>min</sub> c/s	I <sub>max</sub> c/s	I <sub>mean</sub> c/s
Outburst 1				
EIS	–/0.14	–/56	–/63	–/60
BS	15.1	583	3057	2164
IS	0.10	200	220	209
Outburst 2				
EIS	–	–	–	–
BS	30.96	1213	2694	1778
IS	–	–	–	–
Outburst 3				
EIS	–	–	–	–
BS	38.95	1227	6175	4656
IS	–	–	–	–
Outburst 4				
EIS	6.02/2.03	110/70	1295/156	650/127
BS	18.05	368	4835	2330
IS	–	–	–	–
Outburst 4'				
EIS	63	77	530	340
BS	–	–	–	–
IS	–	–	–	–
Outburst 5				
EIS	6.54/1.33	87/128	1444/255	542/203
BS	41.53	810	8555	4925
IS	0.01	458	463	460

EIS: extreme island, BS: banana, IS: island

The left (right) values correspond to the rise (decay)  
of the outburst

TABLE 2  
DURATION IN DAYS OF THE SPECTRAL TRANSITIONS. THESE VALUES SHOULD BE CONSIDERED AS UPPER LIMITS  
AS THEY INCLUDE OBSERVATIONAL GAPS

Transition	Outburst 1	Outburst 4	Outburst 5
EIS→BS	–	2.63	4.94
BS→EIS	4.83	1.06	2.64
BS→IS	1.89	–	0.98
IS→EIS	2.84	–	1.64

TABLE 3

BOUNDARIES AND PROPERTIES OF THE COLOR REGIONS ON WHICH THE TIMING ANALYSIS WAS PERFORMED

States	$(SC, HC)_1$	$(SC, HC)_2$	$(SC, HC)_3$	$(SC, HC)_4$	Mean $SC$	Mean $HC$	Mean Count Rate <sup>a</sup> (c/s)	Number of power spectra	$\chi^2$ (dof)
EISrise1	(0.89,1.08)	(1.12,1.08)	(0.89,1.25)	(1.11,1.26)	1.01	1.14	185	54	122/92
EISrise2	(1.14,1.06)	(1.21,1.07)	(1.14,1.15)	(1.26,1.14)	1.18	1.09	925	34	105/84
EISrise3	(1.19,1.04)	(1.34,1.05)	(1.23,1.10)	(1.29,1.11)	1.25	1.07	1063	23	95/87
EISdecay1	(1.01,1.02)	(1.11,1.03)	(1.00,1.12)	(1.11,1.23)	1.05	1.07	183	37	87/92
EISdecay2	(0.92,1.11)	(1.11,1.14)	(0.88,1.43)	(1.06,1.45)	0.98	1.24	76	40	106/92
EISO4 <sub>1</sub> <sup>t</sup>	(0.96,1.04)	(1.24,1.06)	(0.96,1.26)	(1.10,1.26)	1.05	1.15	188	152	106/87
EISO4 <sub>2</sub> <sup>t</sup>	(1.08,1.04)	(1.07,1.06)	(0.96,1.26)	(1.10,1.26)	1.14	1.14	356	367	114/84
IS	(0.97,0.71)	(1.11,0.89)	(0.82,0.97)	(0.95,1.05)	0.98	0.90	255	28	99/91
BS1	(0.83,0.47)	(0.93,0.41)	(0.89,0.59)	(0.95,0.57)	0.91	0.50	1275	313	193/87
BS2	(0.93,0.41)	(0.99,0.40)	(0.95,0.57)	(1.01,0.57)	0.97	0.49	2086	368	139/89
BS3	(0.99,0.40)	(1.04,0.41)	(1.01,0.57)	(1.02,0.57)	1.02	0.49	3507	368	100/88
BS4	(1.04,0.41)	(1.10,0.42)	(1.02,0.57)	(1.05,0.61)	1.07	0.50	5248	381	89/88
BS5	(1.01,0.42)	(1.18,0.50)	(1.05,0.61)	(1.09,0.68)	1.12	0.51	5315	250	99/88

<sup>a</sup>Background subtracted count rate for the five PCU and bandwidth 2–16 keV

TABLE 4  
POWER SPECTRAL PARAMETERS. ERRORS ARE  $1\sigma$  ( $\Delta\chi^2 = 1$ )

State <sup>a</sup>	$L_{LVLFN}$	$L_{HVLFN}$	$L_b$	$L_{b_2}$	$L_h$	$L_\ell$	$L_{hHz}, L_u$
Characteristic frequency $\nu_{\max}$ (Hz)							
EISrise1	-	-	$0.10 \pm 0.01$	-	$0.59 \pm 0.07$	$12.1 \pm 1.0$	-
EISrise2	-	-	$0.44 \pm 0.02$	-	$2.62 \pm 0.06$	$21.6 \pm 0.9$	$233 \pm 23$
EISrise3	-	-	$0.61 \pm 0.01$	-	$5.4 \pm 0.2$	$32 \pm 2$	$273 \pm 24$
EISdecay1	-	-	$2.3 \pm 0.3$	-	$17 \pm 3$	-	$1160^b$
EISdecay2	-	-	$0.47 \pm 0.05$	-	-	-	$880 \pm 250$
EISO4 <sub>1</sub> '	-	-	$0.130 \pm 0.006$	-	$1.11 \pm 0.07$	$10.8 \pm 0.8$	$180^b$
EISO4 <sub>2</sub> '	-	-	$0.284 \pm 0.009$	-	$2.17 \pm 0.04$	$17.9 \pm 0.6$	$223 \pm 17$
IS	-	-	$20 \pm 2$	-	-	-	$700 \pm 40$
BS1	$0.0130 \pm 0.0007$	$0.36 \pm 0.11$	$62 \pm 5$	$42 \pm 2$	-	$861 \pm 6$	-
BS2	$0.0144 \pm 0.0009$	$0.20 \pm 0.02$	$73 \pm 5$	$45 \pm 5$	-	-	-
BS3	$0.0160 \pm 0.0009$	$0.25 \pm 0.01$	$76 \pm 3$	$24 \pm 3$	-	-	-
BS4	$0.0133 \pm 0.0007$	$0.27 \pm 0.01$	$73 \pm 4$	$16 \pm 1$	-	-	-
BS5	$0.0103 \pm 0.0010$	$0.25 \pm 0.01$	$65 \pm 6$	$13 \pm 1$	-	-	-
Integrated fractional rms <sup>c</sup>							
EISrise1	-	-	$14.8 \pm 0.7$	-	$16.1 \pm 0.6$	$19.2 \pm 0.5$	-
EISrise2	-	-	$13.6 \pm 0.3$	-	$15.8 \pm 0.6$	$16.1 \pm 0.6$	$11.4 \pm 0.4$
EISrise3	-	-	$11.9 \pm 0.4$	-	$18.2 \pm 0.5$	$10.0 \pm 1.0$	$12.2 \pm 0.8$
EISdecay1	-	-	$9.5 \pm 0.6$	-	$13.3 \pm 0.7$	-	$19 \pm 2$
EISdecay2	-	-	$11.0 \pm 0.4$	-	-	-	$38.5 \pm 0.5$
EISO4 <sub>1</sub> '	-	-	$16.0 \pm 0.4$	-	$15.9 \pm 1.0$	$17.9 \pm 1.0$	$17.8 \pm 1.9$
EISO4 <sub>2</sub> '	-	-	$14.9 \pm 0.2$	-	$14.9 \pm 0.5$	$17.3 \pm 0.6$	$14.0 \pm 0.8$
IS	-	-	$15.7 \pm 0.5$	-	-	-	$17 \pm 2$
BS1	$3.19 \pm 0.06$	$0.89 \pm 0.07$	$< 1.3$	$5.0 \pm 0.2$	-	$5.4 \pm 0.2$	-
BS2	$3.44 \pm 0.05$	$1.48 \pm 0.04$	$< 1.2$	$3.4 \pm 0.1$	-	-	-
BS3	$3.49 \pm 0.05$	$1.76 \pm 0.03$	$< 1.4$	$2.3 \pm 0.1$	-	-	-
BS4	$3.33 \pm 0.06$	$1.97 \pm 0.02$	$< 1.1$	$1.79 \pm 0.06$	-	-	-
BS5	$3.29 \pm 0.11$	$2.10 \pm 0.02$	$< 1.0$	$1.55 \pm 0.06$	-	-	-
Q value							
EISrise1	-	-	$0^b$	-	$0^b$	$0^b$	-
EISrise2	-	-	$0^b$	-	$0.42 \pm 0.05$	$0.19 \pm 0.07$	$0.48 \pm 0.15$
EISrise3	-	-	$0^b$	-	$0.16 \pm 0.05$	$0.49 \pm 0.15$	$0.43 \pm 0.16$
EISdecay1	-	-	$0^b$	-	$0^b$	-	$0^b$
EISdecay2	-	-	$0^b$	-	-	-	$0^b$
EISO4 <sub>1</sub> '	-	-	$0.14 \pm 0.04$	-	$0.22 \pm 0.09$	$0.15 \pm 0.13$	$0^b$
EISO4 <sub>2</sub> '	-	-	$0.03 \pm 0.02$	-	$0.33 \pm 0.04$	$0.16 \pm 0.06$	$0.25 \pm 0.13$
IS	-	-	$0.11 \pm 0.09$	-	-	-	$1.9 \pm 0.9$
BS1	$0^b$	$0^b$	$0^b$	$5^b$	-	$7 \pm 1$	-
BS2	$0^b$	$0^b$	$0.16 \pm 0.08$	$3.5^b$	-	-	-
BS3	$0^b$	$0^b$	$0.23 \pm 0.09$	$2.9 \pm 1.2$	-	-	-
BS4	$0^b$	$0^b$	$0.29 \pm 0.07$	$2.4 \pm 1.1$	-	-	-
BS5	$0^b$	$0^b$	$0.41 \pm 0.08$	$2.6 \pm 1.7$	-	-	-

<sup>a</sup>Refers to the regions defined in the color-color diagram (see Table 3)

<sup>b</sup>Fixed

<sup>c</sup>Upper limits are at 95% confidence level

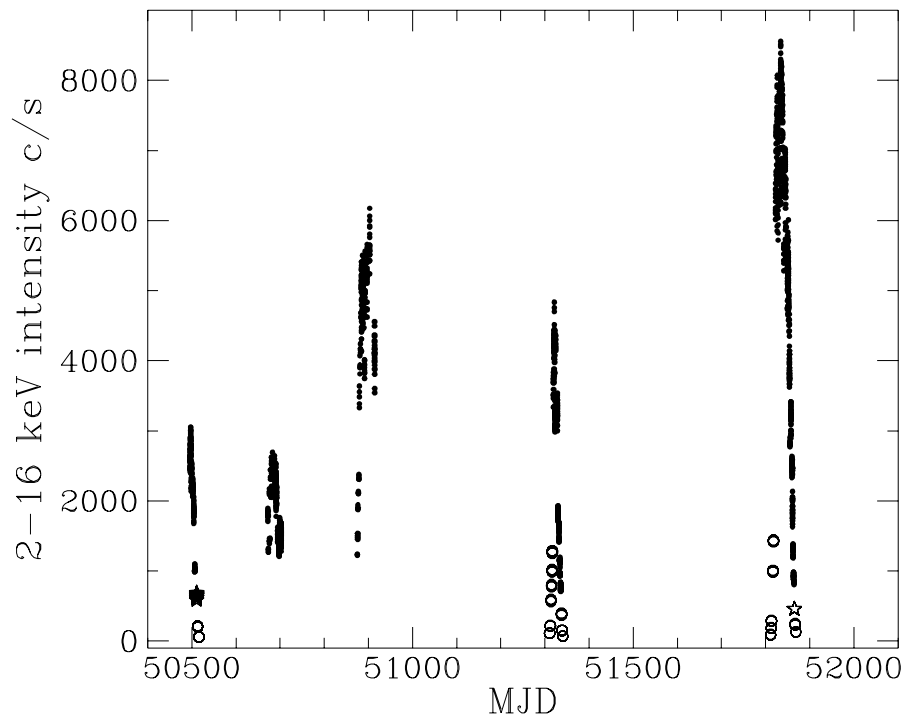


Fig. 1.— Light curve of the entire set of observations showing the five X-ray outbursts. Different symbols represent different spectral states: extreme island (circles), island (stars) and banana (dots).



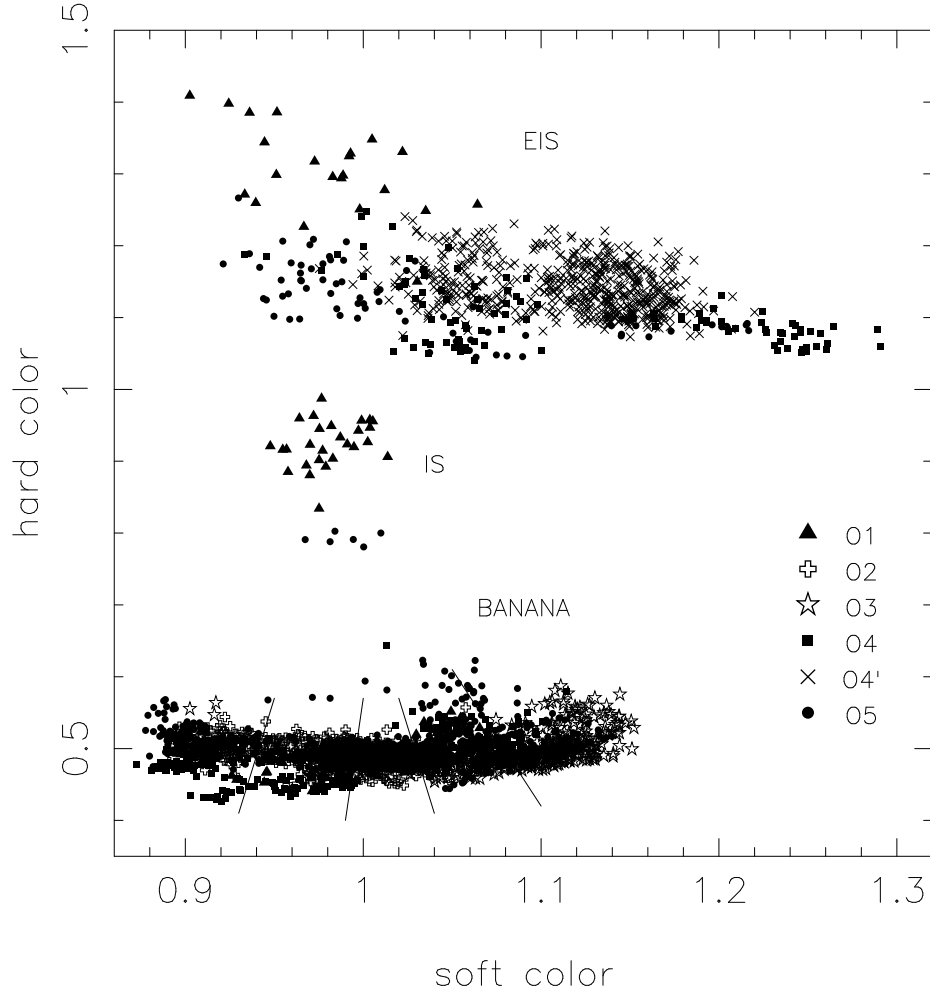


Fig. 2.— Color-color diagram of Aquila X - 1. The soft and hard colors are relative to those of the Crab. Each point in the color-color diagram represents 256 s. No error bars are given but all the points shown in this plot have relative errors smaller than 5%. Different symbols represent different outbursts as indicated. The lines separate the banana-state regions (from BS1 in the left to BS5 in the right).

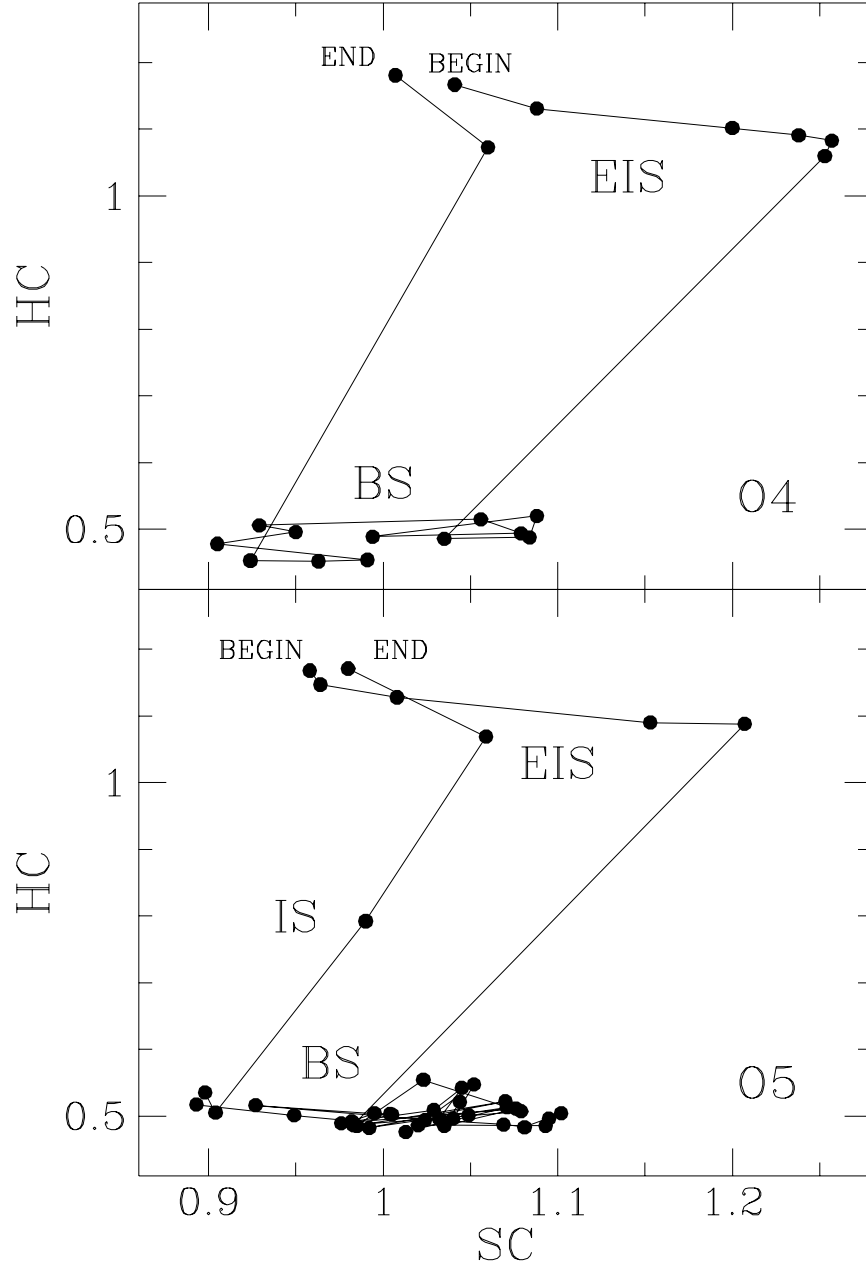


Fig. 3.— Track followed by the source in the color-color diagram during outbursts 4 and 5. Each data point is a one day average.

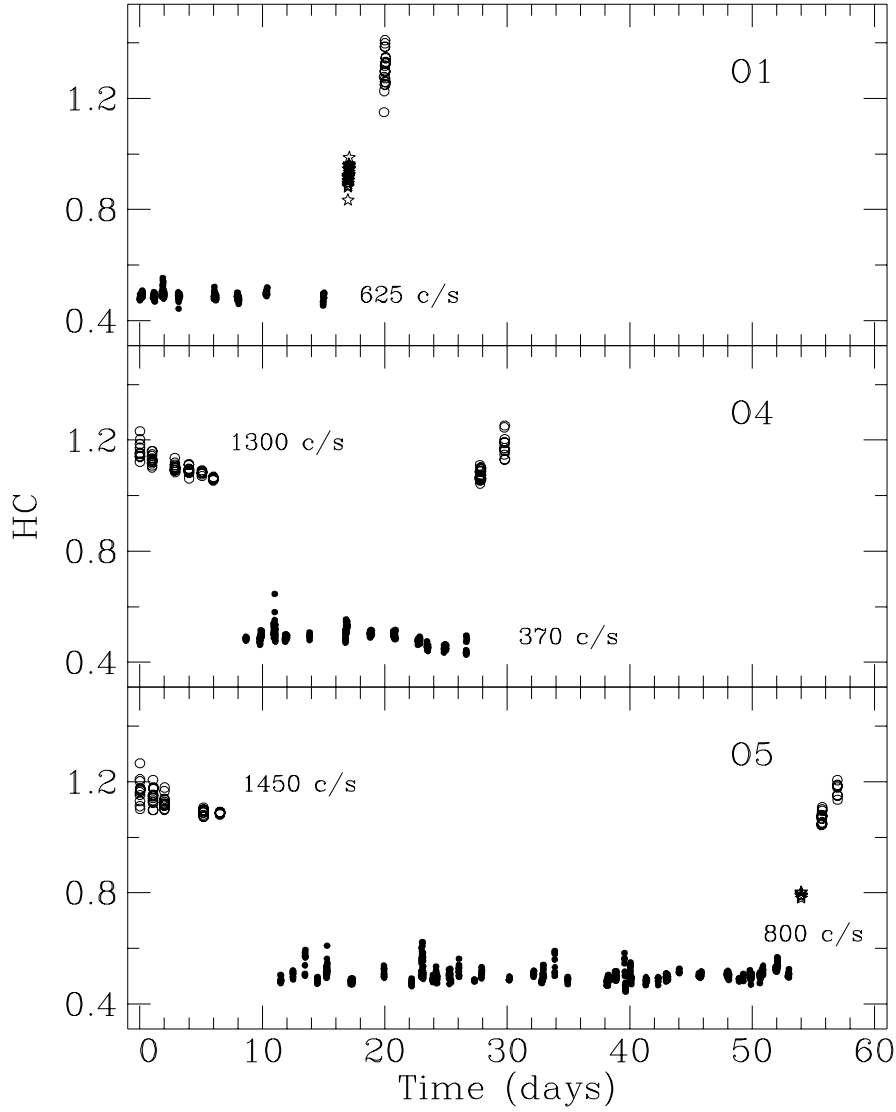


Fig. 4.— Evolution of the hard color showing the transitions between the different spectral states: extreme island (circles), island (stars) and banana (dots). Time refers to the onset of each outburst.

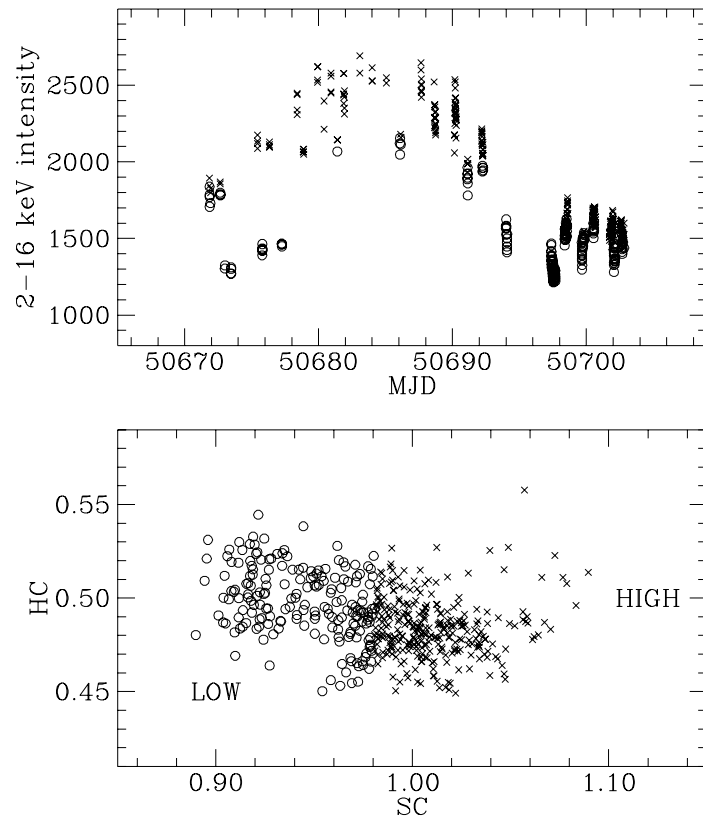


Fig. 5.— Light curve of the second X-ray outburst (upper panel) and the corresponding color-color diagram. The terms *high* and *low* refer to the high-intensity and low-intensity points of the flares.

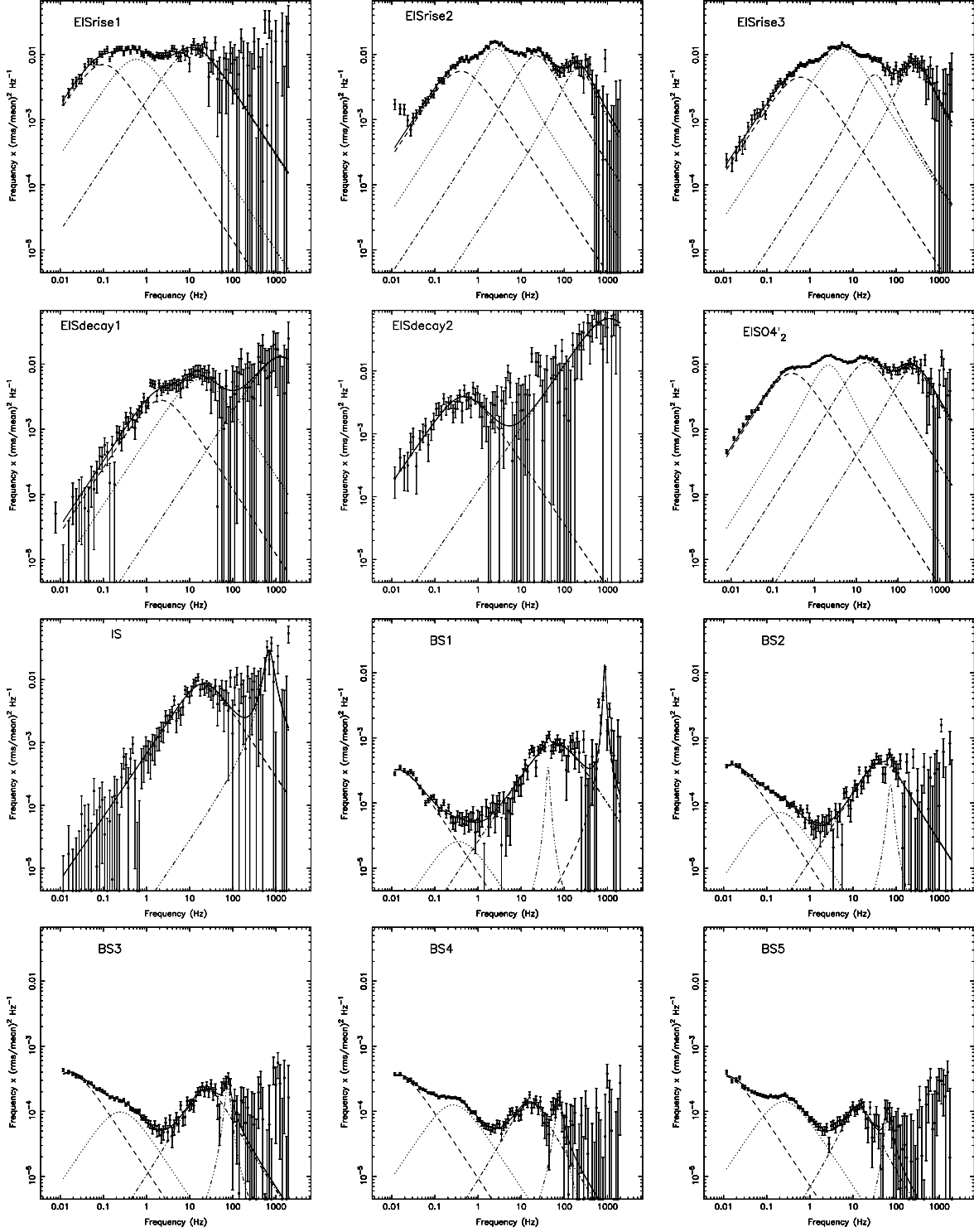


Fig. 6.— Power spectra and best fits for different positions in the color-color diagram (see Table 3) The lines represent the different noise components as follows: for the island states,  $L_b$  (dashed),  $L_h$  (dotted),  $L_\ell$  (dot-dashed) and  $L_u$  (dot-dot-dot-dashed); for the banana state  $L_{LVLFN}$  (dashed),  $L_{HVLFN}$  (dotted),  $L_b$  (dot-dashed),  $L_{b2}$  (dot-dot-dot-dashed). The second dashed line in BS1 corresponds to  $L_\ell$ .

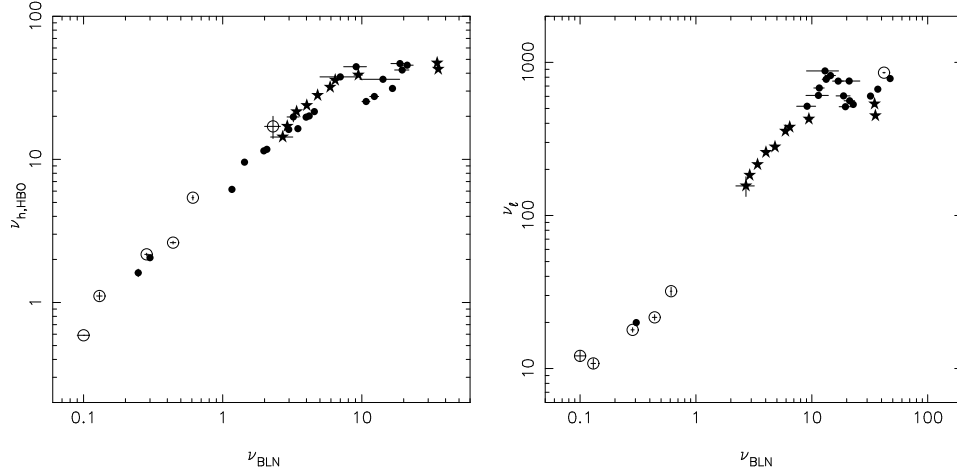


Fig. 7.— Characteristic frequency of the  $L_h$  and  $L_{\ell}$  noise components of the atoll sources 4U 1608–52, 4U 1728–34 and 4U 0614+09 (dots) and the HBO of the Z sources GX 5-1 (stars) as a function of the characteristic frequency of the band-limited noise ( $L_b$  for the atoll sources and HBO for GX5–1). Aquila X – 1 observations have been represented by open circles.

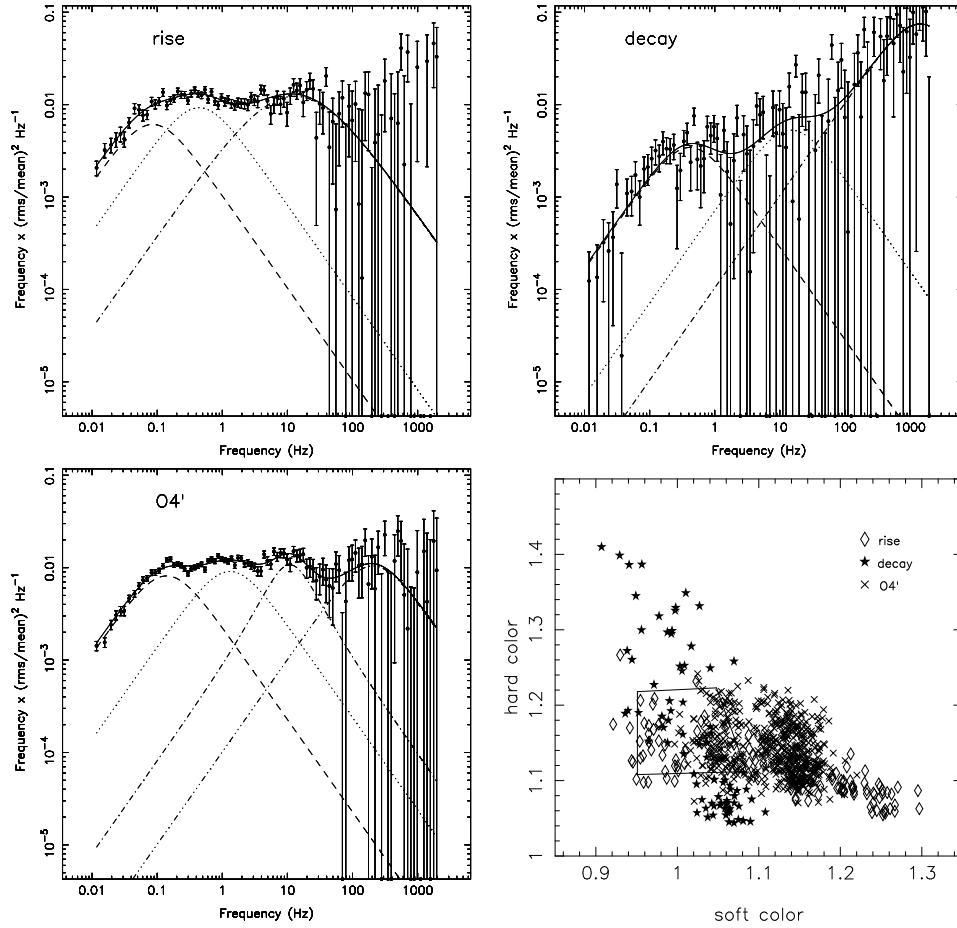


Fig. 8.— Comparison of the power spectra for three different parts of the X-ray outburst. All three power spectra correspond to the same region of the CD. An enlarged view of the island state marking the color region is also plotted.

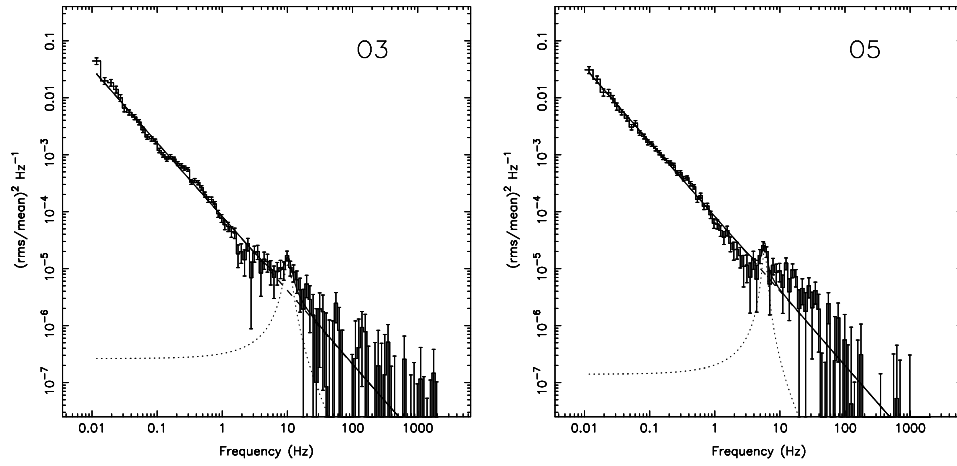


Fig. 9.— N/FBO-like feature in the power spectra of Aquila X – 1 during the peak of outbursts 3 and 5.